

THE EXTRACTION OF THE BEAM OF THE PHILIPS AVF CYCLOTRON

H.L. Hagedoorn and N.F. Verster
Philips Research Laboratories, Eindhoven
(Presented by H.L. Hagedoorn)

The Philips AVF Cyclotron^{1,2,3,4)} is an all-particle cyclotron with a three-sector spiral-ridge field. Its extraction system which shall be described here, is based on the same principle as in the Berkeley 88" Cyclotron⁵⁾. We accelerate through the $\nu_r = 1$ and $\nu_r = 2 \nu_z$ resonances, and deflect the beam with an electrostatic channel, the shape and the efficiency of which are acquired by a graphical analysis of computed orbits.

Particles will be accelerated as far as the field isochronism permits and extracted at a radius well beyond the resonances. The extraction system uses two separate electrostatic channels, as shown in Fig. 1 of paper I-7, p 43. Each channel has four adjustments for shaping them according to the shape of the orbit. The maximum deflector field for 25 MeV protons is about 50 kV over 5 mm. The beam then just passes the cyclotron yoke. After the second channel the beam traverses about 15 cm of fringe field before entering a 25 cm long horizontally focusing and vertically defocusing magnetic channel. It is about 1,5 mean gaps away from the last turn in the cyclotron, wherefore its influence on the field in this region is negligible.

Three magnetic quadrupole lenses of aperture 5.5 cm are used for focusing the external beam into a spot about 2 m beyond the last lens. The first two are focusing and the third defocusing vertically. Despite their narrow aperture the beam loss is small.

Computer Programmes

To investigate the orbit properties in the extraction region we have available a number of computer programmes²⁾. We use three different sets of differential equations. Set I describes the median plane motion in polar coordinates $r(\vartheta)$, $p_r(\vartheta)$. In set II the linearised vertical motion is described, and the influence of the horizontal on the vertical motion taken into account. Set III describes the small horizontal deviations around a solution of set I. The sets II and III are linear, which has the advantage that solutions can be added to form new solutions.

A general vector solution $X(\vartheta)$ of set III is represented by a linear combination $X(\vartheta) = \lambda_1 X_1(\vartheta) + \lambda_2 X_2(\vartheta)$ of two independent solutions.

Each orbit $R(\vartheta) = \begin{pmatrix} r \\ p \end{pmatrix}$ neighbouring a solution $R_0(\vartheta)$ of set I, is represented by $R(\vartheta) = R_0(\vartheta) + X(\vartheta)$. The r accuracy is illustrated in Fig. 1 where the full line represents the radial difference versus azimuth of two orbits found by integrating

- 229 -

set I, and the dotted curve represents the linear combination $X(\vartheta)$.

In the computer programme the transfer matrix $T(\vartheta)$ is calculated from a prescribed starting position ϑ_0 , i.e. $X(\vartheta) = T(\vartheta) \cdot X(\vartheta_0)$.

We use the following types of programmes²⁾:

Programme P7a determines the revolution frequency, the momentum, the energy and the horizontal and vertical oscillation frequencies as functions of the equilibrium orbit radius. The input is the measured magnetic field.

Programme P7b calculates orbits for particles with a definite momentum through ten revolutions without acceleration (Fig. 4 of Ref. 2) to get a stroboscopic picture in the radial phase plane.

Programme P7c calculates fixed-point coordinates as functions of the particle momentum (Fig. 2).

Programme P7d is used extensively for extraction studies. Here a choice can be made of the orbit equations to be integrated :

- 1) Integration of set I is used for investigating the acceleration through $\nu_R = 1$. The acceleration is simulated by suddenly changing the particle momentum by a constant amount each time it passes the dee gap.
- 2) Integration of set I and set II is used to study the influence of the horizontal on the vertical motion of an accelerated particle at $\nu_R = 2\nu_z$.
- 3) Integration of all three sets is used here to calculate the orbits in the electrostatic channel. A detailed output comprising two independent solutions of set II and two of set III is given. The initial input values are ϑ_0 , $r(\vartheta_0)$, $p(\vartheta_0)$, the particle momentum M , the magnetic field and the perturbation in this field. Acceleration is not included.

Acceleration Through the Resonances

At a radius well before the resonance region we have started a number of particles represented by a grid of points in the radial phase plane (Fig. 3). The central point is the equilibrium orbit at that radius. By a first harmonic in the field or, equivalently, an asymmetric dee gap, the non-linear driving force originating from the $3/3$ sub-resonance may cause this grid to move during its acceleration through the resonance region. In our cyclotron acceleration occurs at two angles 162° apart. Thus we can expect a shift of the grid even with no first harmonic. The first harmonic amplitude which compensates for this is about 1.6 gauss.

From Eq. (11.2) in Ref. 3 we find the maximum shift per turn : $\Delta A \leq \pi(C_1 + DA^2/8)$, where C_1 is the relative amplitude of the first harmonic, D the constant of the non-linear sub-resonance, A the relative amplitude of the radial oscillation, and ΔA the increase per turn of this amplitude. Assuming $C_1 = 2 \cdot 10^{-4}$, $D \approx 3$, $A \approx 10^{-2}$ (1/2 cm in our cyclotron) we find $A \approx 7.4 \cdot 10^{-4}$. For a radius of 50 cm the shift is about 0.4 mm/turn. For a reasonable value of the radial amplitude (0.5 cm) the non-linear driving force is very small with respect to the effect of a first harmonic.

As the radial frequency changes rapidly with radius at $\nu_R = 1$, there will be only a few revolutions in this dangerous region. Thus we may expect a very small increase of the amplitude A . For the compensation of a first harmonic, three harmonic coils are available. These must be excited so that $C_1 = 0$ at $\nu_R = 1$.

In Fig. 4 the coordinate shift due to acceleration through $\nu_R = 1$ for a particle starting on the equilibrium orbit is plotted at one azimuth for several values of C_1 . For $C_1 = 0$ there is still a shift caused by the asymmetric dee gap. After correcting for this with $C_1 = 1.6$ gauss, there remains a small shift, which may be due to other effects, e.g. the electric gap crossing resonance which occurs in three-sector machines⁶). C_1 will in practice be adjusted empirically from the beam characteristics. We can conclude that the $\nu_R = 1$ resonance is not too dangerous.

The particles then cross the $\nu_R = 2\nu_z$ resonance, which is very sensitive to small radial amplitudes. In Ref. 5 equations for the amplitudes of the oscillations in this region are given, together with a condition for the magnetic field and the maximum radial amplitude for acceleration through this resonance. In our cyclotron this condition is satisfied, the value of the second derivative μ'' of the mean field with respect to the radius being sufficiently small ($\mu'' \approx -4$). With these equations a qualitative picture can be made of what will happen.

The vertical motion can be described as $z = Ae^{i\nu_z(\vartheta + \varphi)}F(\vartheta) + \text{compl. conj.}$. The periodic Floquet factor $F(\vartheta)$ can be eliminated by a stroboscopic view at $\nu = \nu_0 + 2\pi k/3$. All particles with the same amplitude A but different phases φ are then found in the vertical phase plane on an ellipse (the eigenellipse), the shape of which follows from $F(\vartheta_0)$.

Due to the acceleration the parameters determining $F(\vartheta_0)$, and thus the shape of the eigenellipse, changes. Far from a resonance this change is adiabatic, i.e. the particles remain on the momentary eigenellipse (see upper part of Fig. 5). In the resonance region the change is essentially non-adiabatic, and particles behave differently according to their phase. After the resonance the parameters again vary adiabatically. The particles now lie, however, each on a different eigenellipse (see lower part of Fig. 5). As a result the cigar-shaped ellipse on which they lie rotates, giving amplitude maxima at a frequency $2\nu_z$ (Fig. 6).

We used programme P7d(2) to study the vertical motion including acceleration along these lines. After the first revolution the vertical eigenellipse is calculated and 12 points chosen 15° apart in phase. After each subsequent revolution the coordinates of these particles are given together with the parameters of the new eigenellipse. The maximum vertical amplitude of the beam, represented by the 12 points, is given every 6° . Thus we can check the assumption of adiabatic conditions at the beginning, and follow the vertical motion through the resonance.

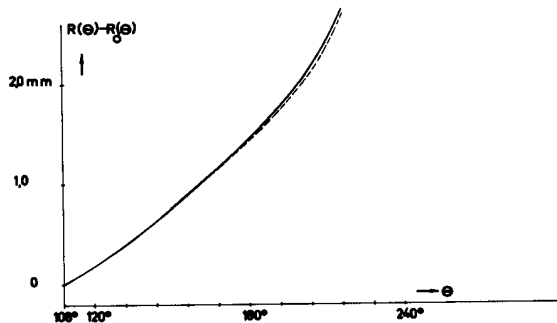


Fig. 1 The full line represents the exact difference between two orbits. The dotted line represents the same difference but calculated by using two independent solutions of the linearized horizontal motion.

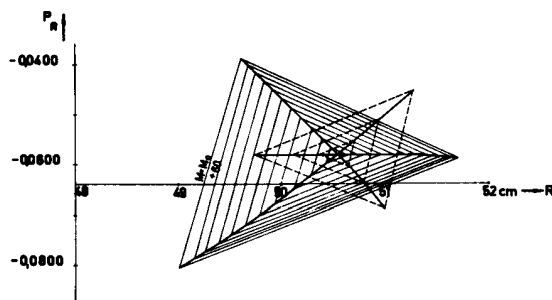


Fig. 2 Variation of stability triangle with increasing momentum in three-sector cyclotron near the outer region where ν_R passes 1. M is the momentum multiplied by 10^5 . $M_0 = 71000$. The momentum step is 60.

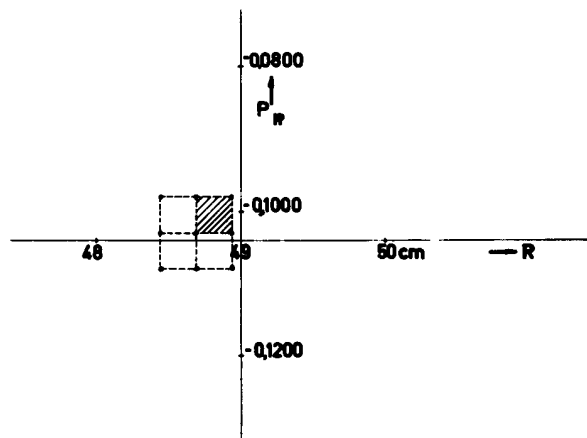


Fig. 3 A grid of initial points in radial phase plane at azimuth θ_0 to be followed through many revolutions by the computer. The central point represents the equilibrium orbit. The momentum of the particles is 0.70397 Wb/m.

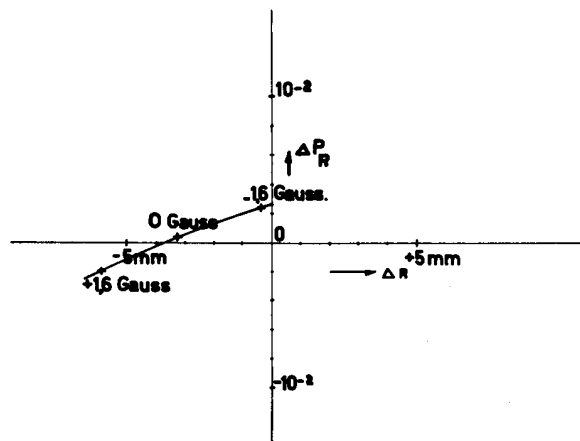


Fig. 4 Coordinate shifts due to traversal of the $\nu_R = 1$ resonance for several values of C . The origin represents the equilibrium orbit. The first harmonic is $C \cos(\theta - 40^\circ)$.

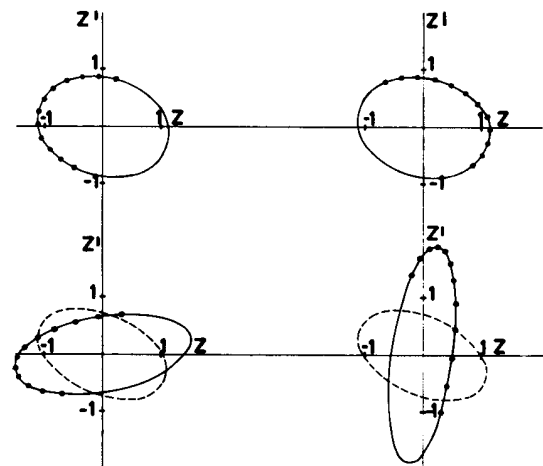


Fig. 5 In the upper case, 12 particles are started on the same vertical eigenellipse (left). To the right they are shown after some time. Both situations are before the resonance region, when parameters still change adiabatically. In the lower set, the same particles, but now shown after the resonance region. The particles now move on different eigenellipses (shown dotted for one particle).

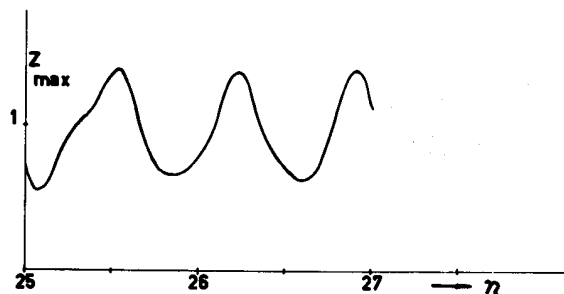


Fig. 6 The vertical beam height z_{max} versus the revolution number n . The vertical frequency $\nu_z = 0.70$

The Extraction of the Beam

A large extraction radius is advantageous because then the required voltage on the electrostatic channel may be relatively low and the particle energy relatively high. The maximum radius depends strongly on the field isochronism. This must be adjusted so that before the extraction region the particles have a positive phase ($+25^\circ$) and at the extraction region a negative phase (-25°) relative to the RF (Fig. 7). The radial frequency at the extraction is well below one.

The digital computer simulates the electric field in the channel by an equivalent magnetic field decrease $\Delta B = V/vd$, where V and d are the channel voltage and gap, and v the particle velocity.

To follow the particles in the channel we have used programme P7d (3), giving all information about the orbit each 6° .

The channel shape is chosen such that the septum and the electrode are parallel to the trajectory of a particle starting on an equilibrium orbit just before the channel entrance. The electric field is chosen such that the particles pass the cyclotron yoke. For 26 MeV protons $V = 52.5$ kV and $d = 5$ mm.

A particle can only be extracted if its trajectory $r(\vartheta)$ does not intersect the inner side $R_{S_1}(\vartheta)$ of the septum and inside the channel lies between the outer side $R_{S_2}(\vartheta)$ of the septum and the HV electrode $R_{S_2}(\vartheta) + d(\vartheta)$, where $d(\vartheta)$ is the channel width. The channel extends from $\vartheta = 108^\circ$ to 216° . Thus the conditions for extraction are : 1) During acceleration : $r(\vartheta) < R_{S_1}(\vartheta)$ for $108^\circ < \vartheta < 216^\circ$, and 2) In the channel : $R_{S_2}(\vartheta) < r(\vartheta) < R_{S_2}(\vartheta) + d(\vartheta)$.

These conditions can be reduced to conditions for the orbit at $\vartheta = 108^\circ$ by a transformation back to this azimuth using the computed transfer matrices. We illustrate this for the geometry of the channel at $\vartheta = 150^\circ$. The aperture (condition 2) is here represented by two vertical lines in phase space (Fig. 8 left); these are transformed back to the channel entrance at $\vartheta = 108^\circ$. The transfer matrices used are calculated in a magnetic field diminished by ΔB to account for the channel electric field.

The inner septum wall is also shown in Fig. 8. This is transformed back to 108° in the sketch at the right (condition 1) using transfer matrices calculated in the proper magnetic field, not decreased by ΔB .

To transform phase space figures over one or more revolutions we have not used the matrix method as it is not sufficiently accurate. Instead a grid (Fig. 3) in phase space was followed during many revolutions. The shadow of the septum walls on subsequent revolutions was found by interpolation between grid points.

In Fig. 9 the channel entrance as well as the beam represented by the grid are shown at 108° for a number of successive revolutions. The beam enters the deflector only at revolutions 29 and 30. For a larger grid, however, more turns will contribute.

The channel apertures for $108^\circ < \vartheta < 216^\circ$ are now transformed back to 108° for the two values of particles momentum corresponding to revolutions 29 and 30. The

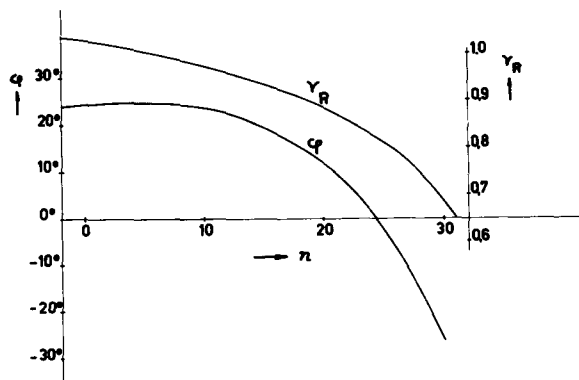


Fig. 7 Phase of particles relative to the RF and radial frequency versus revolution number.

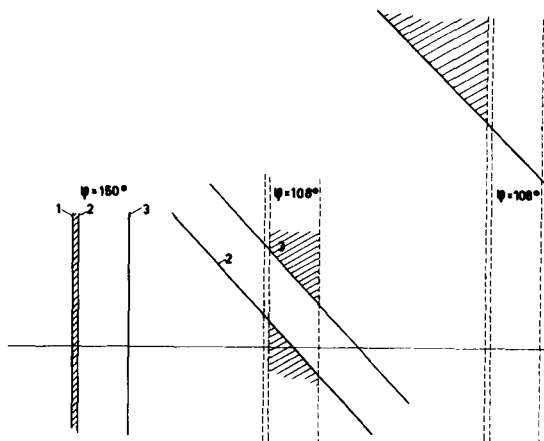


Fig. 8 Left : Geometry of electrostatic channel at $\varphi = 150^\circ$. The inner (1) and outer side (2) of the septum and the HV electrode (3) are shown. The channel aperture is represented by the area between the lines 2 and 3. Centre : The outer septum wall and the electrode transformed back to the channel entrance at 108° . The septum and electrode at 108° are shown by the dotted lines. Only particles between lines 2 and 3 can pass the channel at 150° . Right : The inner septum wall transformed back to 108° . Only particles below the heavy line can be accelerated further.

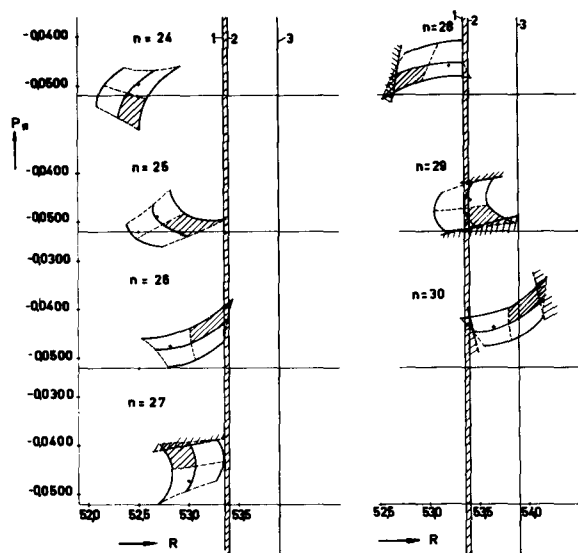


Fig. 9 The phase space grid in Fig. 3 followed during many revolutions. Revolutions 24 to 30 are shown at $\varphi = 108^\circ$. The septum and electrode positions are shown (see Fig. 8). The septum shadow at $n = 26$ and $n = 28$ is represented in the subsequent revolutions by broken lines. The septum shadow at $n = 29$ is given in Fig. 10.

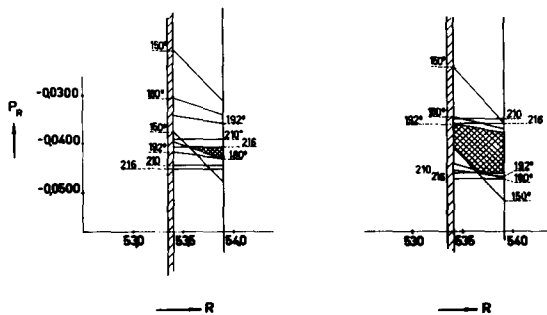


Fig. 11 Left : Channel optimized for highest energy. Low-energy channel aperture is constructed giving small efficiency relative to Fig. 10. Right : Channel readjusted for low energy, giving good extraction efficiency.

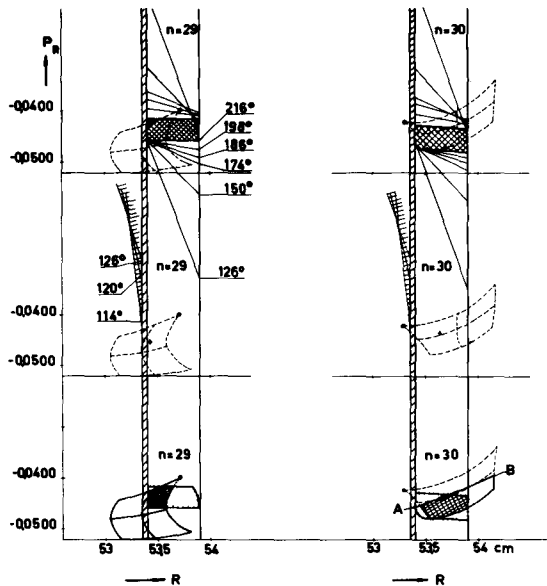


Fig. 10 Upper : The aperture of the channel at several azimuths ($108^\circ < \varphi < 216^\circ$) transformed back to the entrance at 108° for revolutions 29 and 30. The shaded area is the aperture of the whole channel. The beam is represented by the dotted lines. Middle : The inner septum wall transformed back to 108° for revolutions 29 and 30. The shaded area represents particles which will hit the septum. Lower : Shaded areas represent beam going through the channel. The channel aperture is given by the marked lines. The shadow of the septum at $n = 29$ is represented by the line AB in the $n = 30$ diagram. For simplicity the shadows from other turns have been omitted. From Fig. 9 it is clear that they result in only a small loss of beam intensity.

common area of these represents the aperture of the whole channel. This is the shaded area in Fig. 10 upper. Also the inner septum wall is transformed back to 108° (Fig. 10 middle). It is clear that no significant part of the beam strikes the septum internally.

The phase plane diagram of revolution 29 shows the part of the beam being deflected and the part being accelerated further. The latter is transformed to the diagram for revolution 30 (see lower sketch in Fig. 10). The total phase plane area of beam traversing the channel gives the deflector efficiency.

The method has the advantage that it easily determines the part of the beam striking the electrode or septum at a certain place. Moreover, one immediately sees how the channel must be shaped to get a high efficiency. In most cases we find that it should flare out somewhat at the end, decreasing the electric field. However, a limit to this is set by the deflection requirements. For lower energies the deflection voltage will not be too high, leaving a greater freedom to vary the channel shape. Due to magnetic saturation effects, there is in a variable-energy machine a deviation of the lower energy orbits relative to those for higher energies. One may expect that the low-energy extraction efficiency would be very low. This is illustrated by the very small shaded area (efficiency) in Fig. 11 left, calculated for a lower field than in Fig. 10. To eliminate this difficulty we have built in four position adjustments for each channel. If correctly adjusted a sufficient efficiency can be acquired also for lower energies (Fig. 11 right).

Due to the rather low value of the radial frequency at extraction ($\nu_R = 0.75$), there may be a large turn separation for particles which are not well centred. This enhances the extraction efficiency. With 0.5 mm septum thickness and a distance between successive equilibrium orbits of 2 mm, one should expect about 25% loss. In fact it is about 10% or less, due to the above mentioned effect. However, due to the excitation of the vertical oscillations at $\nu_R = 2\nu_z$, this useful radial oscillation has to be small ($< 1/2$ cm).

If the phase plane area of the beam is large, the channel efficiency will be small and the energy spread large. In Fig. 12 the efficiency is plotted as a function of the radial beam extent.

The expected beam spread and divergence after the second electrostatic channel are 0.7 cm and 1° horizontally and 0.5 cm and -1.5° vertically. Since

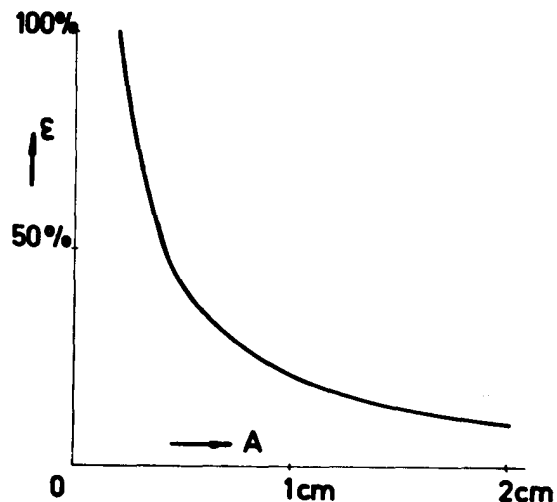


Fig. 12 The channel efficiency ϵ versus the horizontal spread of the beam. A is the radial extent of the initial beam in Fig. 3.

- 235 -

the beam must still traverse some fringe field the divergence will increase. To reduce this we have included the magnetic channel with positive field index. The beam finally leaving the cyclotron has a 1 cm horizontal spread and practically no divergence, and a vertical spread and divergence of 1 cm and 3° . We expect about 80% of the beam leaving the cyclotron to be focused in a spot about 2 m beyond the last of the three quadrupoles mentioned earlier.

References

- 1) N.F. Verster et al., Nucl. Instr. and Meth. 18-19, 88 (1962).
- 2) N.F. Verster and H.L. Hagedoorn, Nucl. Instr. and Meth. 18-19, 327 (1962).
- 3) H.L. Hagedoorn and N.F. Verster, Nucl. Instr. and Meth. 18-19, 201 (1962).
- 4) N.F. Verster et al., See paper I-7.
- 5) A.A. Garren et al., Nucl. Instr. and Meth. 18-19, 525 (1962).
- 6) M.M. Gordon, Nucl. Instr. and Meth. 18-19, 268 (1962).

DISCUSSION

BERKES : Would you please explain in a little more detail in terms of Q_r and Q_z , the most important resonances you are crossing?

HAGEDOORN : $Q_r = 1$ is the most important because even a first harmonic as small as 1 gauss can give a 20 or 30% beam loss.

BERKES : Did you cross the $Q_z = 1/3$ resonance without losses?

HAGEDOORN : Once. Our extraction is at a place where Q_z about equals Q_r , somewhat smaller.

GORDON : Have you considered the use of a small field bump to improve the extraction?

HAGEDOORN : We have not considered that, but we have tested some first harmonics in our cyclotron; for example, with a first harmonic of 20 gauss at different azimuthal positions the beam was immediately lost.

TICKLE : You mention roughly a 1 gauss tolerance for crossing through the $\nu_r = 1$ resonance. Is that with your full dee voltage?

HAGEDOORN : Yes. We have a rather low dee voltage.

WALKINSHAW : Why did you change from resonant extraction?

HAGEDOORN : We made a calculation for the magnetic bump but the coils would be large and difficult to place within the narrow gap of the cyclotron. We were glad to see the possibility of electrostatic extraction.